

X-ray active galactic nuclei in the core of the Perseus cluster

S. Santra^{*}, J. S. Sanders[†] and A. C. Fabian

Institute of Astronomy, Madingley Road, Cambridge. CB3 0HA

29 October 2018

ABSTRACT

We present a study of the X-ray emission from the nuclei of galaxies observed in the core of the Perseus cluster in a deep exposure with *Chandra*. Point sources are found coincident with the nuclei of 13 early-type galaxies, as well as the central galaxy NGC 1275. This corresponds to all galaxies brighter than $M_B = -18$ in the *Chandra* field. All of these sources have a steep power-law spectral component and four have an additional thermal component. The unabsorbed power-law luminosities in the 0.5–7.0 keV band range from 8×10^{38} – 5×10^{40} erg s^{−1}. We find no simple correlations between the K band luminosity, or the FUV and NUV AB magnitudes of these galaxies and their X-ray properties. We have estimated the black hole masses of the nuclei using the K band M_{BH} – L_{Kbol} relation and again find no correlation between black hole mass and the X-ray luminosity. Bondi accretion onto the black holes in the galaxies with mini-haloes should make them much more luminous than observed.

Key words: X-rays: galaxies — galaxies: clusters: individual: Perseus.

1 INTRODUCTION

X-ray observations with the *Chandra* observatory have enabled detailed studies to be made of the X-ray emission of early-type galaxies. The results show hot diffuse gas and low mass X-ray binaries (LMXB), many of which are associated with globular clusters (Sarazin et al 2001; Kim et al 2004a; Fabbiano & White 2003). The hot gas has a temperature of 10^7 K and is not expected to survive in the cores of rich clusters of galaxies, where it should be rapidly depleted by stripping and/or conduction (Gunn & Gott 1972). However, small confined regions, of radius a few kpc, do survive in some early-type galaxies near the centres of rich clusters, as discovered in *Chandra* observations of the Coma cluster by Vikhlinin et al (2001). Yamasaki et al (2002) later found two small galaxy coronae in the centre of the A1060 cluster. Sun et al (2005a) and Sun et al (2005b) found four such X-ray minicorona in A1367 and one in the Perseus cluster, respectively, and Fujita, Sarazin & Sivakoff (2006) found one in A2670. A systematic search for X-ray mini-haloes in 157 early-type galaxies and 22 late-type galaxies in 25 hot, rich nearby clusters by Sun et al (2007) yielded many more examples. From all these observations the authors have concluded that the diffuse hot coronae are stripped from the galaxies in the cores of rich clusters of galaxies, but mini-haloes remain at the centres of some galaxies. Such mini haloes have typical sizes of 1–3 kpc, gas densities of 0.1 cm^{-3} or more and temperatures of about 10^7 K.

Other studies include Finoguenov et al (2004) who measured the X-ray luminosity function of galaxies in the Coma cluster using *XMM-Newton*, and Finoguenov & Miniati (2004) who studied the

impact of high pressure cluster environment on the X-ray luminosity of Coma galaxies. *Chandra* X-ray observations of galaxies in an off-center region of the Coma cluster were done by Hornschemeier et al (2006) to explore the X-ray properties and luminosity function of normal galaxies. They detected 13 galaxies. The X-ray activity is suppressed with respect to that of the field, indicating a lower level of X-ray emission for a given stellar mass.

Some nuclei of nearby early-type galaxies are active but often at a level well below that expected from Bondi accretion of the hot coronal gas (Fabian & Canizares 1988; Di Matteo et al 2000, 2001, 2003; Pellegrini 2005). There are two possible explanations for the low luminosities of nearby black holes: (1) any accretion proceeds at extremely low rates or (2) the accretion occurs at low radiative efficiencies as predicted, for example, by advection-dominated accretion flow (ADAF) models (e.g., Rees et al 1982; Narayan & Yi 1995; Abramowicz et al 1995) and by jet models (e.g. Allen et al 2006).

Here we study the X-ray point sources coincident with member galaxies in the Perseus cluster using a very deep, 900 ks, *Chandra* image. The Perseus cluster is the brightest cluster in the Sky in X-rays, which makes looking for faint or diffuse emission difficult, particularly in the core where our observations are best. In this paper we have looked at X-ray point sources coincident with bright galaxies. We are interested here in the unresolved point sources with power-law spectra, coincident with the galactic nuclei, in order to assess the level of nuclear activity. Sun et al (2007) have previously used the same *Chandra* image of the Perseus cluster, and *Chandra* images of several other clusters, to explore the incidence and general properties of mini-haloes in cluster galaxies. Martini et al (2006) found that 5 per cent of the galaxies brighter than $M_B < -20$ in rich clusters are active, with X-ray luminosity $L_X > 10^{41}$ erg s^{−1}. This is 5 times more than found in optical spec-

^{*} E-mail: sumita@ast.cam.ac.uk

[†] E-mail: jss@ast.cam.ac.uk

Table 1. Point sources obtained from the *Chandra* data which have an optical counterpart. The sources are split into two groups, those on the central CCD, and those on other CCDs. Each section is sorted in RA. Positions use J2000 coordinates.

N	RA	Dec	Nearest galaxy name from NED (J200)
1	03 ^h 19 ^m 26.73 ^s	+41°32′26.0″	NGC 1273
2	03 ^h 19 ^m 40.57 ^s	+41°32′55.2″	NGC 1274
3	03 ^h 19 ^m 51.50 ^s	+41°34′24.8″	NGC 1277
4	03 ^h 19 ^m 54.13 ^s	+41°33′48.4″	NGC 1278
5	03 ^h 19 ^m 59.05 ^s	+41°28′46.5″	NGC 1279
6	03 ^h 20 ^m 00.91 ^s	+41°33′13.8″	Vzw 339
7	03 ^h 19 ^m 17.68 ^s	+41°38′37.8″	2MASX J03191772+4138391
8	03 ^h 19 ^m 34.22 ^s	+41°34′50.0″	CGCG 540-101
9	03 ^h 19 ^m 37.38 ^s	+41°37′58.9″	2MASX J03193743+4137580
10	03 ^h 20 ^m 06.19 ^s	+41°37′46.3″	NGC 1281
11	03 ^h 20 ^m 21.42 ^s	+41°38′23.9″	MCG+07-07-070
12	03 ^h 20 ^m 50.60 ^s	+41°35′57.7″	2MASX J03205074+4136015
13	03 ^h 20 ^m 57.71 ^s	+41°30′20.4″	2MASX J03205776+4130229

troscopic studies by Dressler et al (1985). Our results are consistent with all galaxies above that optical magnitude limit having detected central X-ray sources, albeit at lower luminosities.

This paper is organised as follows: In Section 2 we describe the data preparation, source detection and the X-ray spectral analysis. We compare the X-ray properties with the K band luminosity, UV AB magnitude, radio and black hole mass in Section 3. In Section 4 we discuss our results and summarise them in Section 5.

2 DATA ANALYSIS

2.1 Observations

The 13 *Chandra* observations analysed here are detailed in Fabian et al (2006). Each observation used the ACIS-S3 detector as the aimpoint. The total maximum effective exposure time was 890 ks, after flares were removed. The level 2 event files were reprocessed with ACIS_PROCESS_EVENTS using the acisD2000-01-29gain_ctiN0003.fits gain file, and reprojected to match the coordinate system of the 04952 observation.

The regions of the sky with the highest effective *Chandra* exposure time are shown in Fig. 1. The off-axis effective exposure decreases away from the centre of the ACIS-S3 CCD (which is the SW part of the right region, with a total exposure time of 890 ks). In the NE and NW part of the right chip the exposure times are 75 per cent and 50 per cent of the maximum respectively. The exposure time declines to 13 per cent of the maximum in the region indicated by source 13.

2.2 X-ray source detection

We found 49 X-ray sources by eye in the total *Chandra* 0.3–7 keV image. Of those sources, 13 have optical counterparts. The positions of these 13 sources and the nearest galaxy are listed in Table 1. The sources are split into six close to the central galaxy (detected on the central CCD) and seven further away (detected by other CCDs). The remaining 36 sources without optical counterparts are shown in Table 2. We exclude these sources from the remainder of our analysis.

We detected X-ray sources for all the galaxies brighter than

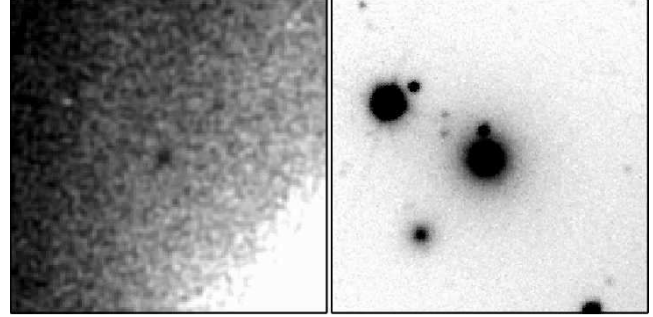


Figure 2. 0.3–1.2 keV X-ray image of PGC 12443 showing drop in surface brightness due to absorption (left) compared with SDSS I-band image (right). The images measure 1 arcmin vertically.

$M_B < -18$. In this deep observation one might expect to detect galaxies fainter than $M_B > -18$, but the diffuse cluster emission makes the background too high for such work.

The red Digitized Sky Survey (DSS2) was first used to identify possible optical counterparts for the X-ray sources. We then examined archival images from the Sloan Digital Sky Survey (SDSS) and the catalogue of Perseus cluster galaxies by Brunzendorf & Meusinger (1999). Fig. 1 shows the SDSS I band image, indicating the detected X-ray sources with optical counterparts. They are all listed as early-type galaxies in the work of Brunzendorf & Meusinger (1999). We do not detect a three-armed spiral galaxy (UGC 2665, listed in Brunzendorf & Meusinger 1999), which lies between sources 7 and 9 (Fig. 1). This morphology excludes it being an early-type galaxy. Moreover, the velocity of this galaxy is 2800 km s^{-1} higher than for the Perseus cluster core, so it is likely an outlier.

In Fig. 3 we show the X-ray contours for each of the detected sources (from a 0.3–7 keV image), overlaid on optical images of the galaxies from SDSS. The first six sources are nearer to NGC 1275 than the others. It is seen that in each of these cases the contours coincide with the nucleus of the galaxy, so the X-ray sources match the optical sources. They are also consistent with being point sources. The remaining seven sources are further from the central galaxy. Some of these distant sources appear off-centred with respect to the optical galaxy centres. However, the offsets for these weak sources are only about 2 arcsec, similar to the offsets obtained for *Chandra* off-axis sources by Kim et al (2004b). They are mainly due to the off-axis point spread function (PSF) having a complex extended shape. The count rate and distance of the galaxies from the central galaxy are given in Table 3.

One galaxy is seen in absorption (Fig. 2). This is listed as 284 or PGC 12443 in the Table of Brunzendorf & Meusinger (1999). It lies midway between galaxies 4 and 5 in Fig. 1 and is centred at $03^{\text{h}}19^{\text{m}}55.6^{\text{s}}$, $+41^{\circ}31'23''$ and is listed as an elliptical galaxy 1.9 magnitudes fainter than NGC 1278. A spectral fit shows that the absorption corresponds to an intrinsic column density of $\sim 3 \pm 1 \times 10^{20} \text{ cm}^{-2}$.

2.3 X-ray spectral analysis

We extracted and modeled the X-ray spectra of those sources identified as Perseus core galaxies. For those sources on the central CCD, we used an extraction region of 3 arcsec. This increased to 5–10 arcsec on the other chips. Spectra for each source were extracted from each of the separate observations and added together. The local backgrounds were extracted from annuli with outer radii

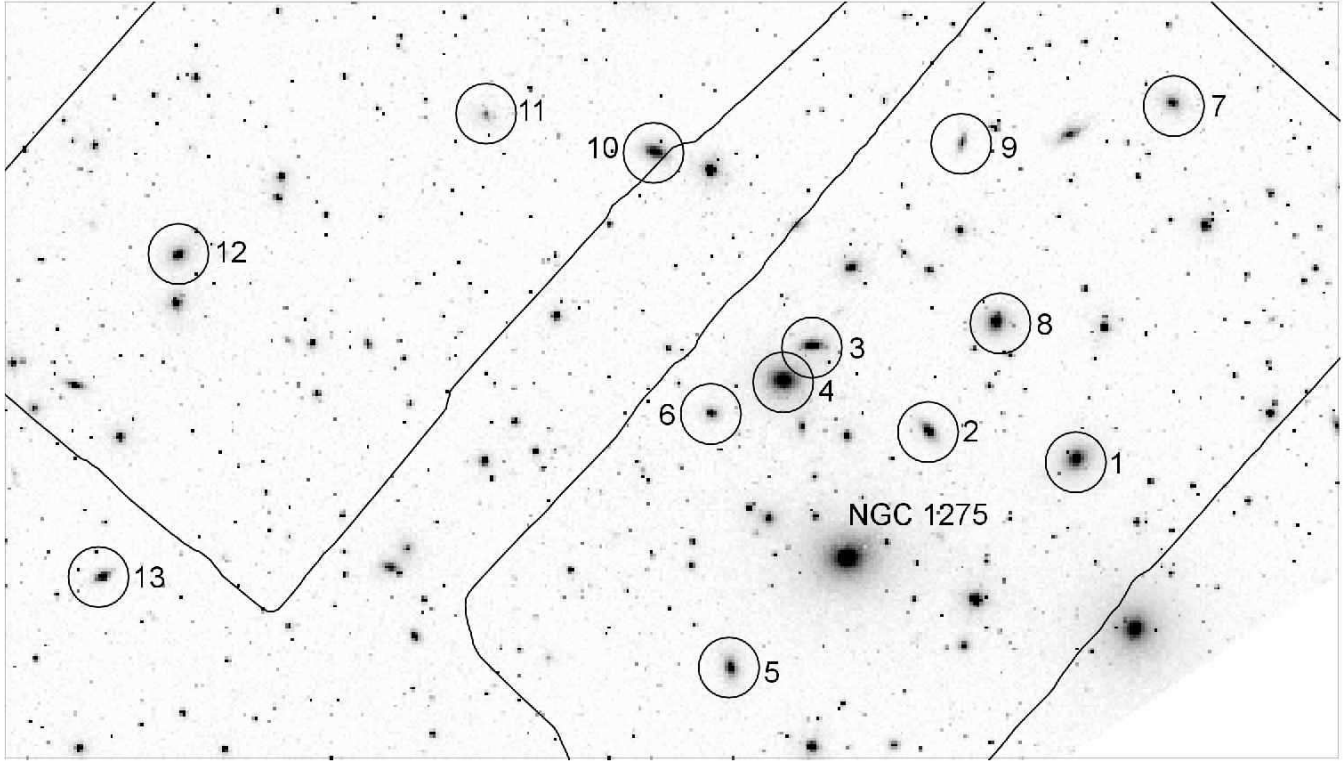


Figure 1. Optical images of the detected X-ray sources from SDSS (numbered according to Table 1). The two regions with greater than 25 per cent of the maximum *Chandra* exposure time are shown by the black contour (each region measures 8 arcmin across).

Table 2. Point sources excluded from further analysis since they have no cluster galaxy counterpart. Fluxes are in $\text{erg cm}^{-2} \text{s}^{-1}$ in the 0.5-7 keV band. They were measured by fitting absorbed powerlaws and MEKAL components (when necessary) to the spectra in the 0.5 to 7 keV band.

RA	Dec	Flux	RA	Dec	Flux	RA	Dec	Flux
03 ^h 19 ^m 09.52 ^s	+41°34' 29.2"	1.1×10^{-14}	03 ^h 19 ^m 30.02 ^s	+41°40' 12.3"	2.3×10^{-14}	03 ^h 19 ^m 48.24 ^s	+41°32' 49.7"	9.6×10^{-16}
03 ^h 19 ^m 11.97 ^s	+41°33' 53.1"	4.5×10^{-15}	03 ^h 19 ^m 30.69 ^s	+41°35' 04.1"	9.5×10^{-15}	03 ^h 19 ^m 51.44 ^s	+41°31' 51.0"	3.7×10^{-15}
03 ^h 19 ^m 15.76 ^s	+41°34' 38.3"	3.2×10^{-15}	03 ^h 19 ^m 33.81 ^s	+41°29' 55.9"	3.3×10^{-15}	03 ^h 19 ^m 56.09 ^s	+41°33' 15.4"	1.3×10^{-14}
03 ^h 19 ^m 15.95 ^s	+41°34' 07.9"	7.8×10^{-16}	03 ^h 19 ^m 35.67 ^s	+41°27' 49.9"	1.7×10^{-15}	03 ^h 19 ^m 59.91 ^s	+41°39' 36.1"	5.1×10^{-15}
03 ^h 19 ^m 19.93 ^s	+41°31' 56.2"	5.0×10^{-15}	03 ^h 19 ^m 37.49 ^s	+41°38' 44.2"	2.0×10^{-14}	03 ^h 20 ^m 01.50 ^s	+41°31' 27.5"	2.5×10^{-14}
03 ^h 19 ^m 20.10 ^s	+41°37' 46.4"	2.1×10^{-14}	03 ^h 19 ^m 38.37 ^s	+41°27' 53.5"	1.3×10^{-15}	03 ^h 20 ^m 02.71 ^s	+41°30' 33.3"	9.0×10^{-16}
03 ^h 19 ^m 21.12 ^s	+41°31' 19.4"	6.2×10^{-14}	03 ^h 19 ^m 43.68 ^s	+41°27' 25.1"	2.2×10^{-15}	03 ^h 20 ^m 04.76 ^s	+41°38' 39.5"	5.1×10^{-15}
03 ^h 19 ^m 22.26 ^s	+41°39' 37.3"	4.4×10^{-15}	03 ^h 19 ^m 43.91 ^s	+41°33' 04.7"	5.2×10^{-15}	03 ^h 20 ^m 05.34 ^s	+41°30' 54.5"	4.3×10^{-15}
03 ^h 19 ^m 23.64 ^s	+41°37' 08.7"	3.6×10^{-14}	03 ^h 19 ^m 44.10 ^s	+41°25' 53.2"	1.6×10^{-14}	03 ^h 20 ^m 11.52 ^s	+41°36' 59.4"	6.1×10^{-15}
03 ^h 19 ^m 25.00 ^s	+41°31' 32.2"	1.2×10^{-15}	03 ^h 19 ^m 45.47 ^s	+41°42' 19.5"	6.0×10^{-15}	03 ^h 20 ^m 14.31 ^s	+41°36' 05.8"	4.8×10^{-15}
03 ^h 19 ^m 25.13 ^s	+41°40' 26.5"	1.3×10^{-14}	03 ^h 19 ^m 46.27 ^s	+41°37' 35.7"	7.4×10^{-14}	03 ^h 20 ^m 18.24 ^s	+41°37' 24.0"	2.8×10^{-15}
03 ^h 19 ^m 28.11 ^s	+41°34' 25.4"	3.0×10^{-15}	03 ^h 19 ^m 47.75 ^s	+41°27' 23.5"	7.7×10^{-16}	03 ^h 20 ^m 19.69 ^s	+41°37' 30.8"	5.8×10^{-15}

of 5 arcsec on the central CCD, increasing to 10-20 arcsec on the other chips. Response matrix files (RMF) and ancillary response files (ARF) were created for each of the sources by averaging the RMFs and ARFs from the individual observations (created using MKACISRMF and MKWARF).

The spectral fitting was performed using XSPEC v11.3.2. The spectra were grouped to have a minimum of 20 counts in each spectral bin before background subtraction in order to use the χ^2 statistic. Model fitting was carried out in the 0.5 – 7.0 keV band.

Each X-ray spectrum was fitted by a power-law with possible intrinsic absorption and then, separately, by a MEKAL thermal spectrum. Most were best fitted by the power-law spectrum. We let the power-law slope (Γ) and the absorbing column density

(N_H) vary freely. In some cases the column density was less than $1.3 \times 10^{21} \text{ cm}^{-2}$ (the galactic absorption value) which was unphysical, so we fixed it at this minimum. The photon indexes of sources 5, 8 and 9 were fixed at 2.0. In the cases where a single component power-law did not give a satisfactory fit, a MEKAL component with a temperature fixed at 0.6 keV was added to improve the fit. We assume that this is a mini-halo component, although it is not spatially resolved.

The results of the spectral fitting of all the galaxies are given in Table 3. The values of N_H and Γ vary between $(1.3 - 3.7) \times 10^{21} \text{ cm}^{-2}$ and $(2.0 - 3.77)$ respectively. The values of column density was fixed at the minimum for sources 1, 2, 6, 9, 10, 11,

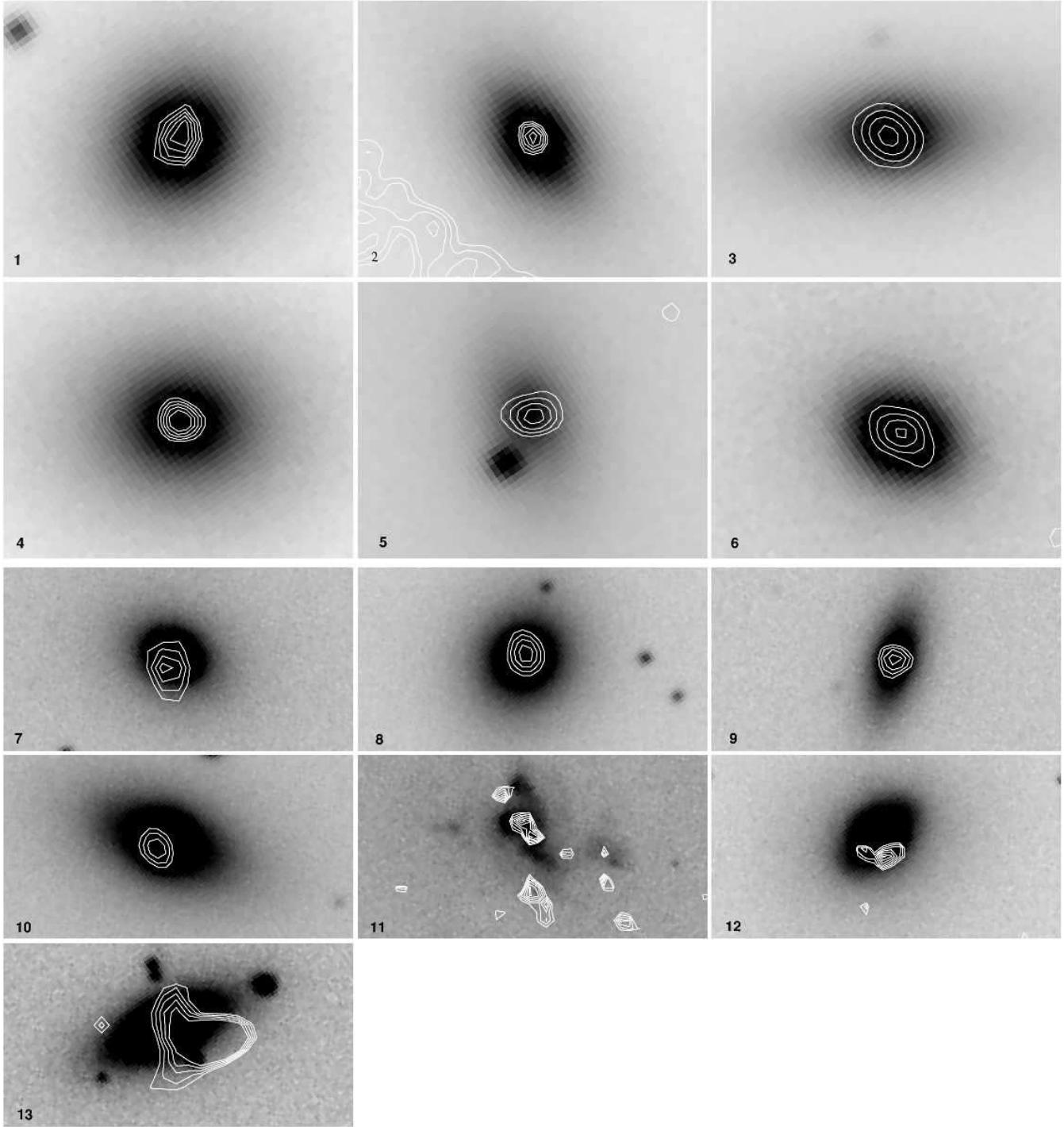


Figure 3. X-ray contours for each of the sources with optical counterparts, overlaid on the SDSS I band optical images. The first six sources are nearer to the central galaxy and the rest are further away. The first six images are $27.8'' \times 16.5''$ in size, the next seven are $55.2'' \times 23''$.

12 and 13. The Γ values are much steeper than for LMXB (Irwin, Athey & Bregman 2003).

A typical spectral fit (for source 3) is shown in Fig. 4. The spectrum was fitted using an absorbed power-law and MEKAL model.

In Table 4, the $0.5 - 7.0$ keV flux and the absorption corrected luminosities of the individual sources based on the best-fitting absorbed power-law model, and in some cases MEKAL+absorbed

power-law model, are presented. Luminosities were determined assuming a redshift 0.018 and cosmological model with $H_0 = 70 \text{ km s}^{-1} \text{ Mpc}^{-1}$. The distances of all of these galaxies are assumed to be the same as that of NGC 1275, as they are in the same cluster (Brunzendorf & Meusinger 1999). The uncertainties on the X-ray luminosities were determined by generating a Monte Carlo Markov Chain using the built-in XSPEC functionality. After the chain had converged, we calculated the luminosity (with-

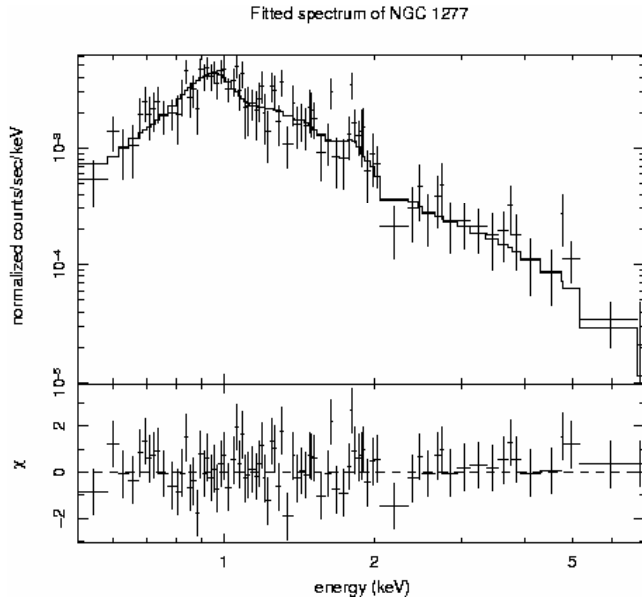


Figure 4. The X-ray spectrum of source 3 showing the best-fit absorbed power-law + MEKAL (solid line). The fit residuals are presented in the lower panel.

out absorption) from each set of values in the chain. The quoted luminosity is the median luminosity from the chain, and the uncertainties were calculated using the 15.85 and 84.15 percentiles. The rest-frame 0.5 – 2 keV luminosities of thermal minihaloes of Perseus core galaxies from Sun et al (2007) are also given in Table 4. These are the total (power-law+MEKAL) luminosities. Sun et al (2007) give no data for sources 6, 7, 9, 11, 12, 13 and found only two minihalo objects. We found two more. The absolute total B band magnitudes of the galaxies are also shown in Table 4, calculated using the luminosity distance and the total B band flux density from NED. There are no reported B band fluxes for sources 5, 6, 11, 12, 13.

As the first 200 ks of the observations occurred around 2 yr before the remainder, we investigated whether the detected sources were time variable. We determined the X-ray flux of the sources for the two epochs of observation and found the fluxes were the same within the uncertainties. Therefore no significant variability was found.

3 PROPERTIES OF THE EARLY-TYPE GALAXIES

We now make a systematic investigation of the properties of the detected 13 early-type galaxies.

3.1 K band luminosity and X-ray luminosity

In Fig. 5 we plot for each source the unabsorbed power-law X-ray luminosity versus the K band luminosity. L_K was derived from K_{20} measured within the 20 mag arcsec⁻² isophote (taken from Two Micron All Sky Survey, 2MASS), using $M_{K\odot} = 3.33$ mag. We also plot a straight line showing the linear relation between the X-ray luminosity of LMXB in a galaxy and the galaxy K band luminosity (from Kim & Fabbiano 2004). Kim & Fabbiano (2004) find a range in K band luminosity of 7 to $40 \times 10^{10} L_{K\odot}$, which is a similar range to our galaxies. All but two of our sources lie below the relation.

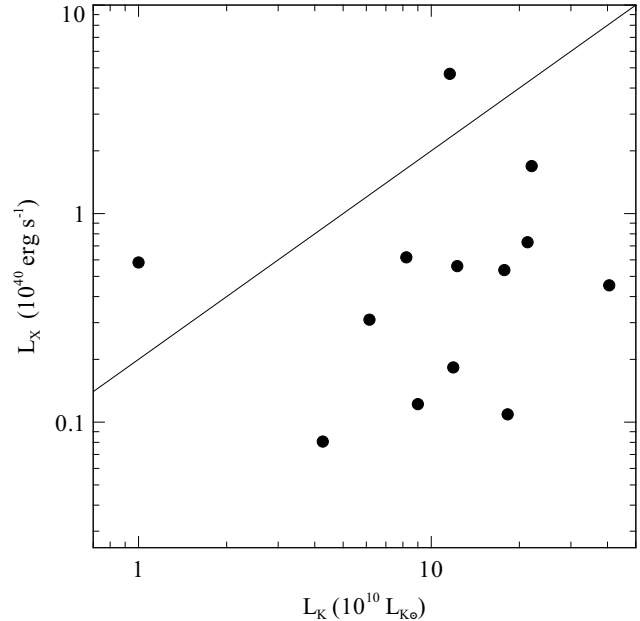


Figure 5. X-ray luminosity vs K band luminosity plot. The straight line is the linear relation between the X-ray luminosity of LMXB and the K band luminosity of a galaxy, taken from Kim & Fabbiano (2004).

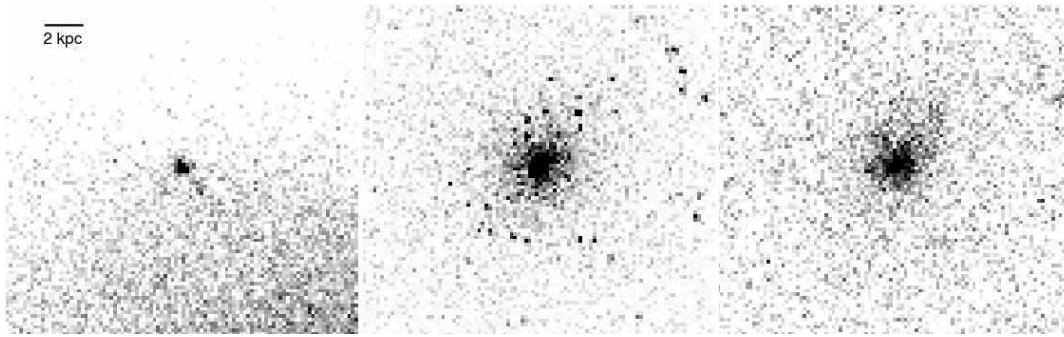
Therefore the galaxies appear superficially underluminous in point sources.

To assess the effect of instrumental effects and projection of intracluster medium on the detectability of point sources, we compared from Perseus NGC 1278 ($L_K = 40.55 \times 10^{10} L_{K\odot}$), the optically brightest galaxy detected here, against the publicly-available *Chandra* observation of NGC 720 ($L_K = 18.58 \times 10^{10} L_{K\odot}$). NGC 720 lies at a distance of 28 Mpc, is not in a cluster and has a *Chandra* observation of 40 ks length (OBSID 492). To account for the effect of distance on the spatial scale, we binned the image of NGC 720 by a factor of 3, and smoothed it by 1 arcsec to account for the PSF at the position of NGC 1278. From this image we subtracted a flat background, then multiplied the image by a factor of 2.3 to account for the difference in exposure time and distance between the Perseus and NGC 720 observations. We added a flat background component to account for the projected intracluster medium in Perseus. Finally we generated an image by making a Poisson realization of our model, to account for counting statistics. We show an image of NGC 1278, NGC 720 before processing, and the final simulated NGC 720 image in Fig. 6.

It is clear that most of the halo of point sources (LMXB) spread several arcmin around NGC 720 become undetectable under the observing conditions of NGC 1278. The situation would become worse after the higher absorption to the Perseus cluster is included. We only detect in NGC 1278 a point source coincident with the nucleus and a possible LMXB to the SW. It would be interesting to see whether this last source coincides with a globular cluster there but we have found no published information of globular clusters in our 13 galaxies. We conclude that the low X-ray luminosity of most of the 13 galaxies, when compared with nearby ones, is due to our inability to resolve the expected, spatially-distributed, population of point sources.

Table 3. Count rate in the energy range between 0.5 – 7.0 keV for the detected galaxies, distance from the central galaxy and best-fitting parameters of the X-ray spectral fits.

N	Count rate (counts ks ⁻¹)	Distance from the central galaxy (arcmin)	Model	$\chi^2/\text{d.o.f}$	N_{H} (10 ²² cm ⁻²)	Γ	kT (keV)
1	4.99 ± 0.08	4.4	Power-law	167.64/144	0.13 (fixed)	2.34 ^{+0.16} _{-0.16}	
2	1.94 ± 0.05	2.6	Power-law	53.08/66	0.13 (fixed)	2.37 ^{+0.31} _{-0.28}	
3	9.12 ± 0.24	3.7	Mekal+	190.57/178	0.30 ^{+0.04} _{-0.04}	2.51 ^{+0.22} _{-0.20}	0.6
4	2.87 ± 0.07	3.3	Power-law	89.79/95	0.19 ^{+0.06} _{-0.07}	2.43 ^{+0.44} _{-0.25}	
5	4.97 ± 0.11	2.8	Mekal+	170.40/147	0.37 ^{+0.14} _{-0.14}	2.0 (fixed)	0.6
6	2.48 ± 0.06	3.5	Power-law	95.46/84	0.13 (fixed)	2.19 ^{+0.24} _{-0.22}	
7	4.10 ± 0.07	9.8	Power-law	124.42/124	0.24 ^{+0.12} _{-0.13}	3.29 ^{+0.89} _{-0.56}	
8	2.97 ± 0.06	4.9	Mekal+	94.28/96	0.24 ^{+0.07} _{-0.07}	2.0 (fixed)	0.6
9	1.63 ± 0.04	7.5	Power-law	61.4/56	0.13 (fixed)	2.0 (fixed)	
10	1.35 ± 0.04	7.8	Power-law	30.21/46	0.13 (fixed)	2.02 ^{+0.22} _{-0.20}	
11	14.89 ± 0.13	9.9	Mekal+	252.16/268	0.13 (fixed)	3.25 ^{+0.66} _{-1.26}	0.6
12	3.21 ± 0.06	12.8	Power-law	106.28/105	0.13 (fixed)	3.77 ^{+0.41} _{-0.38}	
13	3.93 ± 0.07	12.98	Power-law	106.15/124	0.13 (fixed)	2.43 ^{+0.17} _{-0.16}	

**Figure 6.** (Left) NGC 1278 in the Perseus cluster. (Centre) NGC 720 at the same physical scale as NGC 1278. (Right) Simulated image of NGC 720 accounting for projected cluster emission, PSF and Poisson noise.

3.2 UV band magnitudes, radio emission, black hole mass and X-ray luminosity

GALEX FUV and NUV photometry of the centres of the detected Perseus cluster galaxies was taken from O’Connell et al (2007). We plot FUV and NUV AB magnitudes against the unabsorbed power-law X-ray luminosity in Fig. 7. We see that there is no obvious correlation between UV and X-ray fluxes. The FUV and NUV magnitudes vary from 19 – 21.5 and 18 – 20.5 respectively, whereas the X-ray luminosity ranges by almost a factor of 100.

We found only four published values of radio power for the 13 galaxies. These are at 1.4 GHz data and from Miller & Owen (2001) and Sijbring (1993). The values of the logarithm of radio power in W Hz⁻¹ are 21.9, 21.2, 21.5 and 21.2 for CGCG 540-101, NGC 1277, NGC 1278 and NGC 1281, respectively.

The black hole mass of each galaxy was calculated using the relation from Marconi & Hunt (2003), relating M_{BH} and $L_{K,\text{bul}}$ for the ‘Group 1’ galaxies:

$$\log M_{\text{BH}} (M_{\odot}) = (8.21 \pm 0.07) + (1.13 \pm 0.012)(\log L_{K,\text{bul}} - 10.9), (1)$$

where $L_{K,\text{bul}}$ is in units of $L_{K\odot}$. We show in Table 5 the total 2MASS K band luminosities (taken from NED) and the derived black hole mass. The masses vary from 2.4×10^7 to $1.1 \times 10^9 M_{\odot}$.

The unabsorbed power-law X-ray luminosity was plotted against the black hole mass of the galaxies in Fig. 8. The open diamonds show those sources with a minihalo. The distances between the galaxies and the central galaxy, NGC 1275, are also given. We see that all the sources are within 250 kpc radius from NGC 1275. No correlation is found between the X-ray luminosity and the black hole mass.

Table 4. Total fluxes, velocities, absorption corrected luminosities, the rest frame 0.5 – 2 keV luminosities from Sun et al (2007) and total B band magnitude of the sources.

N	Total Flux (0.5 – 7.0 keV) (erg cm ⁻² s ⁻¹)	Velocity (from NED) (km s ⁻¹)	Absorption corrected Luminosity (0.5 – 7.0keV) (erg s ⁻¹)		Rest frame (0.5 – 2 keV) luminosities (erg s ⁻¹) (from Sun et al. 2007)	Total B band luminosity (mag)
			Mekal	Power-law		
1	7.66×10^{-15}	5387		$7.29^{+0.58}_{-0.57} \times 10^{39}$	$< 3.80 \times 10^{39}$	-20.04
2	1.90×10^{-15}	6413		$1.83^{+0.30}_{-0.27} \times 10^{39}$	$< 3.16 \times 10^{39}$	-19.58
3	1.57×10^{-14}	5066	$6.90^{+5.85}_{-2.72} \times 10^{39}$	$1.69^{+0.23}_{-0.18} \times 10^{40}$	4.47×10^{39}	-19.51
4	4.26×10^{-15}	6090		$4.53^{+0.79}_{-1.42} \times 10^{39}$	$< 2.75 \times 10^{39}$	-21.01
5	2.19×10^{-15}	7285	$2.15^{+0.50}_{-0.47} \times 10^{39}$	$1.22^{+0.72}_{-0.64} \times 10^{39}$	$< 3.09 \times 10^{39}$	
6	3.36×10^{-15}	5186		$3.10^{+0.40}_{-0.38} \times 10^{39}$		
7	3.95×10^{-15}	6211		$6.17^{+0.56}_{-0.54} \times 10^{39}$		-18.68
8	3.49×10^{-15}	4500	$4.08^{+1.97}_{-1.33} \times 10^{39}$	$1.09^{+0.70}_{-0.59} \times 10^{39}$	3.16×10^{39}	-18.48
9	9.09×10^{-16}	8574		$8.07^{+3.42}_{-3.26} \times 10^{38}$		-19.56
10	6.55×10^{-15}	4300		$5.83^{+0.57}_{-0.53} \times 10^{39}$	$< 4.37 \times 10^{39}$	-19.29
11	7.8×10^{-15}	3749	$5.50^{+1.36}_{-1.60} \times 10^{39}$	$3.66^{+2.70}_{-2.18} \times 10^{39}$		
12	4.45×10^{-15}	5306		$5.6^{+0.79}_{-0.77} \times 10^{39}$		
13	4.82×10^{-14}	4965		$4.68^{+0.31}_{-0.31} \times 10^{40}$		

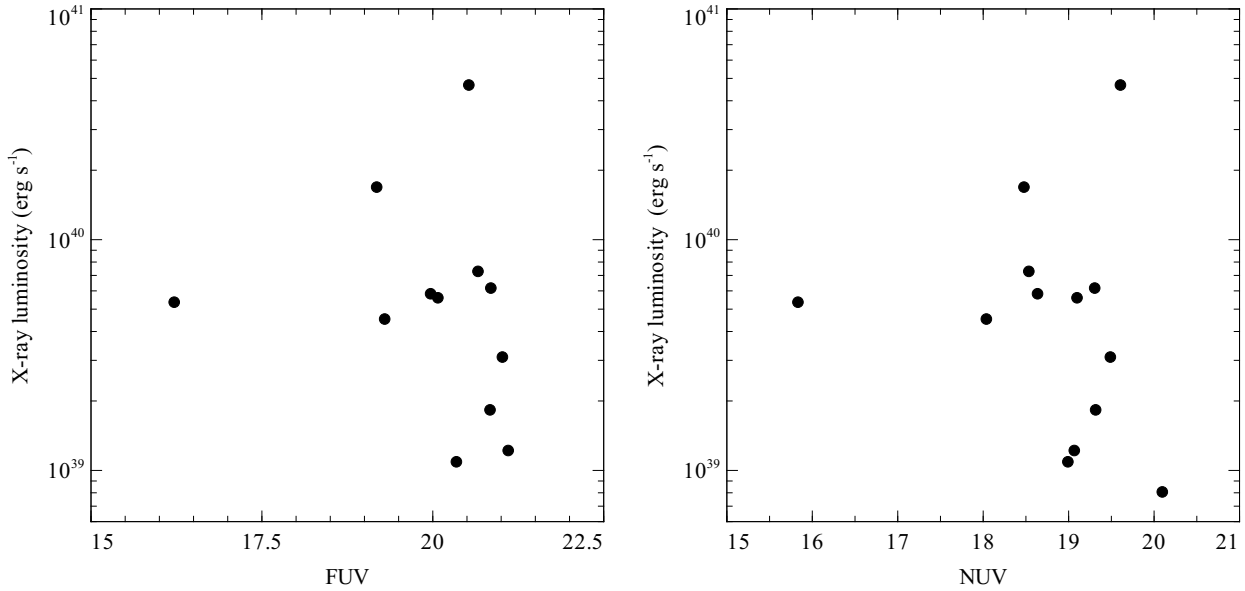
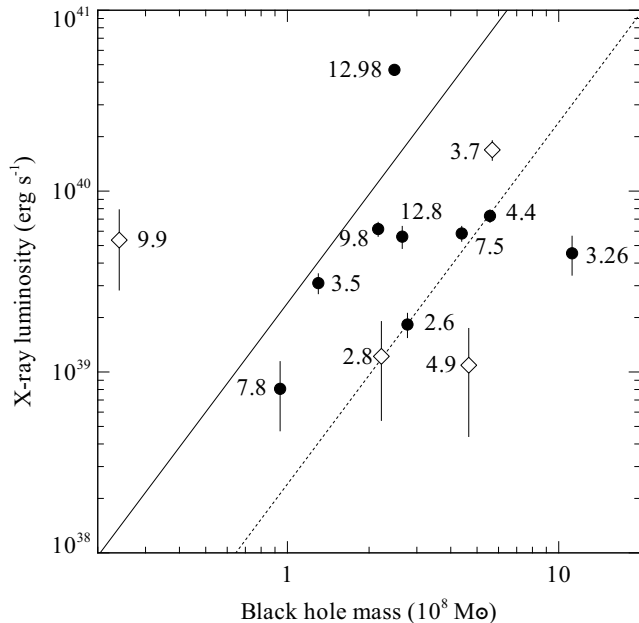
**Figure 7.** Source FUV (left) and NUV (right) AB magnitudes plotted against X-ray luminosity. Note that all sources are essentially at the same distance.

Table 5. Total K band flux density and black hole mass of the galaxies

N	K band flux density ($10^{-28} \text{ W m}^{-2} \text{ Hz}^{-1}$)	Black hole mass ($10^8 M_{\odot}$)
1	7.79	5.58
2	4.21	2.77
3	7.92	5.69
4	14.4	11.2
5	3.44	2.22
6	2.15	1.30
7	3.36	2.16
8	6.61	4.66
9	1.61	0.94
10	6.29	4.31
11	0.48	0.24
12	4.03	2.95
13	3.80	2.48

**Figure 8.** Unabsorbed power-law X-ray luminosity plotted against black hole mass. The numbers are the distance in arcmin between the central galaxy and the detected galaxies. Objects with a minihalo are plotted with an open symbol. The solid line represents the expected bolometric luminosity from Bondi accretion and the dashed line the 0.5–7 keV luminosity (see Section 4).

4 DISCUSSION

All of the bright early-type galaxies in the region studied are detected in X-rays. The X-ray luminosities range from just below $10^{39} \text{ erg s}^{-1}$ to $\sim 5 \times 10^{40} \text{ erg s}^{-1}$ in an unresolved component. The sources are spatially coincident, or consistent within uncertainties, with the centres of the galaxies. The LMXB expected in these galaxies are barely detectable owing to the high background due to the dense intracluster gas.

All 13 sources have a power-law spectral component and 4 have an additional thermal component, suggestive of a mini-halo (as also found by Sun et al 2007). The photon index of the power-law is steeper than typically expected from LMXB ($\Gamma \sim 1.6$; Irwin,

Athey & Bregman 2003), indicating that the sources are unlikely to be central, unresolved, concentrations of LMXB.

The bolometric accretion luminosity expected from Bondi accretion of the intracluster medium in the cluster core, assuming that the galaxy motion is subsonic, is $6 \times 10^{40} \left(\frac{M_{\text{BH}}}{5 \times 10^8 M_{\odot}} \right)^2 \text{ erg s}^{-1}$ (e.g. Allen et al 2006). We assume that the gas has a density of 0.02 cm^{-3} and velocity/sound speed of 10^3 km s^{-1} . With a typical bolometric correction of 10 in the 0.5–7 keV band for sources at low Eddington rate (Vasudevan & Fabian 2007), most of our sources have X-ray luminosities close to that expected from Bondi accretion (Fig. 8), especially when variations in velocity etc. are considered. Where there are mini-haloes, and it is plausible that they all have some form of mini-halo due to central stellar mass loss, then the expected accretion luminosity should be up to 10^3 times higher owing to the gas being much denser and cooler. If these galaxies do contain mini haloes then they are further extreme examples of the general problem found for the supermassive black holes in early-type galaxies (Fabian & Canizares 1988; Pellegrini 2005). On simple grounds they should all be much more luminous than observed if the black hole accretes in a radiatively-efficient manner. None are as faint as our own Galactic Centre, Sgr A*, but there is the fuel at hand for them to be much brighter.

The solution may lie in ADAFs (Narayan & Yi 1995) or other radiatively inefficient flows or with outflows so that little matter reaches the centre (Blandford & Begelman 1999). The luminosity of the sources may also act back on the accreting gas (Ostriker et al. 1976; Di Matteo et al 2003). Alternatively the matter may accrete to the centre and power relativistic jets (e.g. Allen et al 2006), which can be very radiatively inefficient. We do not however see any disturbance in the surrounding hot gas, nor radio emission, which would be expected to accompany such powerful jets.

Our results do not distinguish which solution is the more correct, but underscore the widespread nature of the problem.

5 CONCLUSION

We have made a detailed analysis of X-ray point sources detected with a deep *Chandra* ACIS-S observation of the core of the Perseus cluster. The main observational results and conclusions of our study are:

- (i) We have found a total of 13 X-ray sources coincident with the nuclei of early-type galaxies projected near the centre of Perseus cluster (excluding NGC 1275).
- (ii) All 13 sources have a power-law spectra component and 4 have an additional thermal component.
- (iii) No obvious correlations are found between X-ray luminosities and the K band luminosities, UV AB magnitudes and black hole masses of the galaxies.
- (iv) Our results are consistent with the nuclei of all early-type galaxies in rich clusters being active, albeit at a low level.
- (v) There is no apparent difference between the X-ray luminosities of nuclei in a minihalo compared with those with no detected minihalo. Bondi accretion, for those nuclei with a minihalo, should make them much more luminous.
- (vi) Some form of radiatively-inefficient accretion is likely operating in these sources.

ACKNOWLEDGEMENTS

The authors thank R. O’Connell for the Table of UV fluxes. This research has made use of the NASA/IPAC Extragalactic Database (NED) and Sloan Digital Sky survey (SDSS). ACF thanks The Royal Society for support.

REFERENCES

- Abramowicz M., Chen X., Kato S., Laota J. P., Regev O., 1995, *ApJ*, 483, L37
- Allen S. W., Dunn R. J. H., Fabian A. C., Taylor G. B., Reynolds C. S., 2006, *MNRAS*, 372, 21
- Blandford R. D., Begelman M. C., 1999, *MNRAS*, 303, L1
- Brunzendorf J., Meusinger H., 1999, *A & AS*, 139, 141
- Dressler A., Thompson I. B., Shethman S. A., 1985, *ApJ*, 288, 481
- Di Matteo T., Quataert E., Allen S. W., Narayan R., Fabian A. C., 2000, *MNRAS*, 311, 507
- Di Matteo T., Johnstone R. M., Allen S. W., Fabian A. C., 2001, *ApJ*, 550, L19
- Di Matteo T., Allen S. W., Fabian A. C., Wilson S. A., Young A. J. 2003, *ApJ*, 582, 133
- Fabian A. C., Canizares C. R., 1988, *Nature*, 333, 829
- Fabian A. C., Sanders J. S., Taylor G. B., Allen S. W., Crawford C. S., Johnstone R. M., Iwawawa K., 2006, *MNRAS*, 366, 417
- Fabbiano G., White N. E., 2003, *astro-ph/0307077*
- Fujita Y., Sarazin C. L., Sivakoff G. R., 2006, *PASJ*, 58, 131
- Finoguenov A., Briel U. G., Henry J. P., Gavazzi G., Iglesias-Paramo J., Boselli A., 2004, *A&A*, 47
- Finoguenov A., Miniati F., 2004, *A&A*, 418, L21
- Gunn J. E., Gott J. R., 1972, *ApJ*, 176, 1
- Hornschemeier A. E., Mobasher B., Alexander D. M., Bauer F. E., Bautz M. W., Hammer D., Poggianti B. M., 2006, *ApJ*, 643, 144
- Irwin J. A., Athey A. E., Bregman J. D., 2003, *ApJ*, 587, 356
- Kim D. -W., Fabbiano G., 2004a, *ApJ*, 611, 846
- Kim D. -W., Cameron R. A., Drake J. J., Evans N. R., Freeman P., Gaetz T. J., Ghosh H., Green P. J., Harnden F. R., Jr., Karovska M., Kashyap V., Maksym P. W., Schlegel E. M., Silverman J. D., Tananbaum H. D., Vikhlinin A. A., Wilkes B. J., Grimes J. P., 2004b, *ApJS*, 150, 19.
- Marconi A., Hunt L. K., 2003, *ApJ*, 589, L21
- Martini P., Kelson D. D., Kim E., Mulchaey J. S., Athey A. A., 2006, *ApJ*, 644, 116
- Narayan R., Yi I., 1995, *ApJ*, 444, 231
- O’Connell R. W., Rosario D. J., Schiavon R. P., Conselice C. J., Gallagher J. S., Wyse R. F. G. (in preparation)
- Ostriker J. P., McCray R., Weaver R., Yahil A., 1976, *ApJ*, 208, L61
- Pellegrini S., 2005, *ApJ*, 624, 155
- Rees M. J., Begelman M. C., Blandford R. D., Phinney E. S., 1982, *Nature*, 295, 17
- Sijbring D., 1993, Ph.D. thesis, Univ. Groningen
- Sarazin C. L., Irwin J. A., Bregman J. N., 2001, *ApJ*, 556, 533
- Sun M., Vikhlinin A., Forman W., Jones C., Murray S. S., 2005a, *ApJ*, 619, 169
- Sun M., Jerius D., Jones C., 2005b, *ApJ*, 633, 165
- Sun M., Jones C., Forman W., Vikhlinin A., Donahue M., Voit M., 2007, *ApJ*, 657, 197
- Vasudevan R., Fabian A. C., 2007, *MNRAS*, submitted
- Vikhlinin A., Markevitch M., Forman W., Jones C., 2001, *ApJ*, 555, L87
- Yamasaki N. Y., Oshashi T., Furusho T., 2002, *ApJ*, 578, 833